Molecular scale energy dissipation in oligothiophene monolayers measured by dynamic force microscopy

2009 Nanotechnology 20 434021

(http://iopscience.iop.org/0957-4484/20/43/434021)

Nanotechnology **20** (2009) 434021 (7pp) doi:10.1088/0957-4484/20/43/434021

Molecular scale energy dissipation in oligothiophene monolayers measured by dynamic force microscopy

Nicolas F Martínez[1], Wojciech Kamiński[2,3], Carlos J Gómez[1], Cristiano Albonetti[4], Fabio Biscarini[4], Rubén Pérez[3] and Ricardo García[1]

[1] CSIC-Instituto de Microelectrónica de Madrid (IMM), Isaac Newton 8, E-28760 Tres Cantos, Madrid, Spain
[2] Institute of Experimental Physics, University of Wrocław, plac Maksa Borna 9, PL-50-204 Wrocław, Poland
[3] Departamento de Física Teórica de la Materia Condensada, Universidad Autónoma de Madrid, E-28049 Madrid, Spain
[4] CNR-Istituto per lo Studio dei Materiali Nanostrutturati (ISMN), Via P Gobetti 101, I-40129 Bologna, Italy

E-mail: ruben.perez@uam.es and rgarcia@imm.cnm.csic.es

Received 15 June 2009, in final form 11 August 2009
Published 2 October 2009
Online at stacks.iop.org/Nano/20/434021

Abstract
We perform a combined experimental and theoretical approach to establish the atomistic origin of energy dissipation occurring while imaging a molecular surface with an amplitude modulation atomic force microscope. We show that the energy transferred by a single nano-asperity to a sexithiophene monolayer is about 0.15 eV/cycle. The configuration space sampled by the tip depends on whether it approaches or withdraws from the surface. The asymmetry arises because of the presence of energy barriers among different deformations of the molecular geometry. This is the source of the material contrast provided by the phase-shift images.

(Some figures in this article are in colour only in the electronic version)

1. Introduction

Amplitude modulation atomic force microscopy (AM-AFM) has enabled high resolution imaging of soft materials in their natural environment and state [1–5]. True molecular resolution has also been achieved in ambient conditions [4]. A key feature of AM-AFM is the ability to map simultaneously the shape and the compositional variations of heterogeneous materials. Variation of the phase shift of a vibrating tip across a heterogeneous surface gives rise to a powerful source of spatial contrast. This method is known as *phase-imaging* AFM [5]. Phase-imaging has mapped the crystallization, melting and phase transitions in polymeric materials [6], the motion of structural defects in block-copolymer melts [7] or the morphology of salmonella cells [8]. Phase-imaging has also been applied to identify nanoscale energy dissipation processes [9]. The sine of the phase lag existing between the excitation of the tip and its response to the tip–surface interactions is related to the local energy dissipation on the surface [5, 10, 11]. Imaging methods based on mechanical dissipative processes are not uncommon in force microscopy [12–15]. However, the compatibility of phase-imaging AFM with air and liquid environments, nanoscale resolution and low forces makes this technique widely used in the characterization of soft matter. Phase-shift measurements have been proposed as a new feedback parameter in force microscopy [16–18].

The theory of AM-AFM in air is well understood [19–22]. However, the complexity of the structures resolved by phase-imaging AFM, involving a few thousand atoms, has so far prevented us from linking the observed contrast with atomic and molecular energy dissipating processes.

Sexithiophene (T6) is a widely studied organic semiconductor forming highly ordered crystal domains by high-vacuum sublimation [23, 24]. T6 is treated as a rigid-rod-like molecule in the solid state, and due to this property it is used as a semiconductor for the fabrication of organic thin film transistors. T6 forms densely packed molecular layers with a herringbone arrangement in the so-called low-temperature phase [25, 26]. This crystal structure, slightly contracted in the in-plane lattice parameters and with the molecules standing homeotropic on the substrate, is also observed in monolayer islands at sub-monolayer coverage of silicon oxide up to 6 ML (the so-called thin film phase) [27]. A population of conformers, generated by the rotation of adjacent thienyl groups around the C–C bond, could coexist [28]. As there are five bonds connecting the six thienyl units, it would be possible, in principle, for T6 molecules to dissipate different amounts of energy through its internal rotational degrees of freedom. Therefore, this molecule offers the opportunity to investigate the interplay between intra-molecular, inter-molecular and lattice energy dissipation channels.

Here we identify the molecular processes which are responsible for the contrast observed in phase-imaging AFM by combining experimental measurements with continuum mechanics and first-principles calculations. We first measure the energy transferred by a silicon dioxide tip into a region of T6 molecules to be of 0.18 eV/molecular chain. This value is comparable to the average value (0.15 eV) obtained from first-principles calculations for an indentation of 2 Å. First-principles calculations show that the adhesion hysteresis observed experimentally has its molecular origin in the configuration space of the system. During the approach (loading) the system is trapped, due to the presence of energy barriers, in several configurations that differ from those sampled during the retraction of the tip (uploading). Those configurations correspond to local energy minima. We demonstrate that the energy detected in the experiments performed in ambient conditions is directly related to the molecular properties of T6.

2. Experimental method

The experimental method is based on the measurement of dynamic-dissipation curves with an AFM operating in the amplitude modulation mode [9]. Dynamic-dissipation curves consist of the representation of the average energy transferred by the tip to the sample surface as a function of oscillation amplitude while the tip approaches the surface. The measurements have been performed at room temperature.

T6 molecules have been deposited onto silicon substrates by sublimation in ultra-high vacuum of the polycrystalline material from a Knudsen cell in an organic molecular beam deposition apparatus [23]. Single-beam silicon cantilevers (Nanosensors, Germany) with spring constants k in the 1–10 N m^{-1} range and Q factors in the 100–300 range have been used to perform the experiments. The cantilever is oscillated at its free resonance frequency (∼120 kHz) with a free amplitude A_0 in the 5–15 nm range. All the experiments have been performed in a dry N_2 atmosphere (relative humidity of about 0%). The force constant is determined by characterizing the hydrodynamic response of the cantilever [29].

3. Theoretical methods

3.1. First-principles and molecular dynamics calculations

The calculations are based on density functional theory (DFT) implemented with a local-orbital basis using the FIREBALL code [30]. This code is designed to deal with large-scale simulations and offers a very favourable accuracy-to-efficiency balance provided that the basis set is carefully chosen [31]. Therefore, several tests have been performed to choose the optimized local-orbital basis set, which yields a very good description of the structural properties of both T6 molecules and SiO_2 clusters. The first-principles calculations presented in this paper are performed within the local density approximation (LDA) for the exchange–correlation functional [32]. DFT-LDA calculations provide the theoretical framework to determine the short-range chemical forces that control the molecular scale image contrast. The van der Waals interactions, which due to their long-range character do not contribute significantly to the high resolution spatial contrast, are not included in the calculations.

We consider a silica tip constructed from a very stable SiO_2 cluster [33] with 39 atoms (21 oxygen, 12 silicon and 6 hydrogen atoms; see figures 1(a) and (b)). This model provides the high mechanical stability of the oxide and displays at the apex the protruding doubly coordinated oxygen atoms that are expected on the outer layer of the oxide. The T6 sample is described by a free-standing monolayer of T6 molecules with a 4 × 2 unit cell, with lattice vectors determined from the 2 × 1 surface unit cell (b = 7.70 Å, c = 5.52 Å) measured in x-ray diffraction experiments [27], and which contains eight molecules in the characteristic herringbone pattern (see figure 1(a)). The bottom atoms of each molecule are fixed during the simulations in order to capture the key experimental information for the T6 adsorption on the Si oxide: T6 molecules are standing up normal to the surface and they interact strongly with the substrate. The 4 × 2 unit cell, including the silica tip, involves 393 atoms.

The short-range forces are calculated for each tip–sample distance during the approach and retraction as a thermal average over a molecular dynamics simulation of 2 ps performed in the canonical ensemble at T = 300 K.

3.2. Dynamic AFM simulations with contact mechanics models

Dynamic AFM simulations based on a point-mass model have been performed in order to make contact between the first-principles simulations and the experimental results. The tip–sample interaction includes the Derjaguin–Muller–Toporov (DMT) contact mechanics approximation [34] and long-range attractive forces. Our model, described in detail in [9], assumes different long-range attractive interactions (α_a, α_r) and surface energies (γ_a, γ_r) during approach and retraction in order to

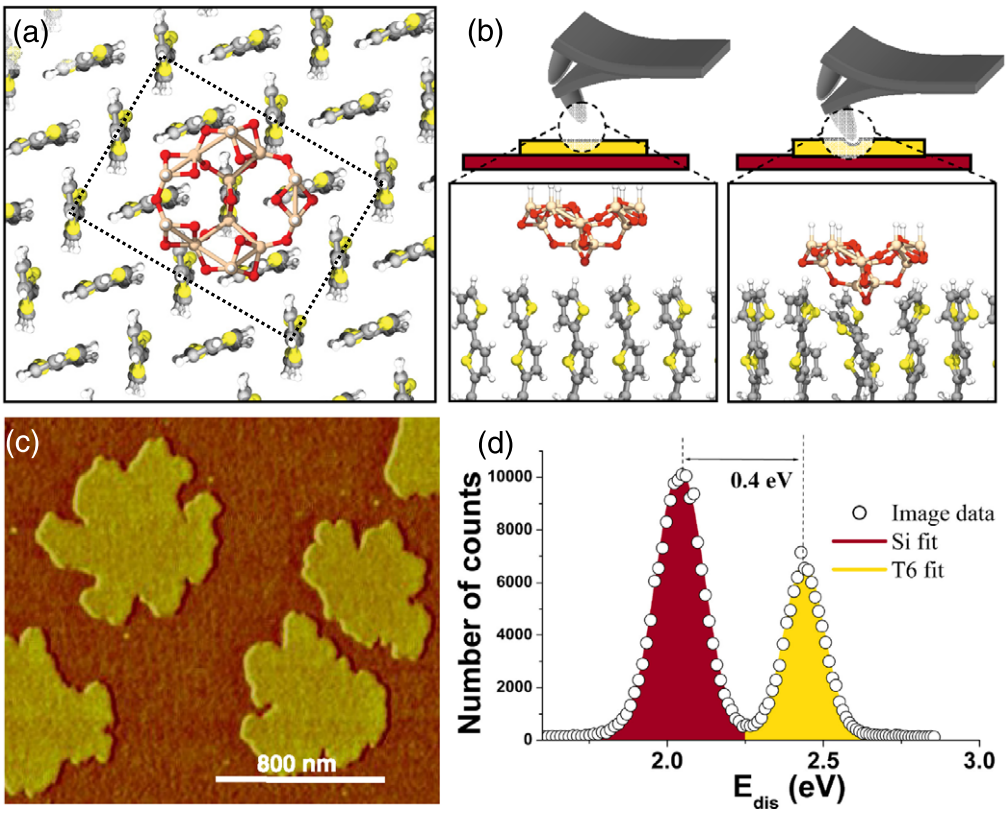

Figure 1. (a) Top view of the herringbone structure and the 4 × 2 unit cell of T6. A single silica tip stands on top of the molecules. (b) Schematic illustration of the tip–T6 interface, presenting results of first-principles simulation of an interaction between a silica tip and the T6 monolayer at two different distances. (c) Phase-imaging AFM image of several T6 monolayer islands deposited on silicon. (d) Energy dissipation histograms extracted from (c). The number of counts is larger on the silicon surface because at the present coverage its surface area is larger. Colour code for the atoms: oxygen (red), sulfur (yellow), carbon (grey), hydrogen (white) and silicon (light salmon).

describe the hysteresis in the force versus distance curves. The attractive force is calculated by the van der Waals expression:

$$F_i = -\frac{\alpha(t)}{d^2} \tag{1}$$

where the strength of the interaction α depends on whether the probe approaches (α_a) or retracts away (α_r) from the surface.

The dynamical parameters of the cantilever (A_0, k and Q) are taken from independent experimental measurements. The parameters in the force model, including the strength of the interactions during approach and retraction and the effective elastic modulus of the interface Y^*, are adjusted to fit a single experimental point (A_i, ϕ_i) in the energy dissipation curves (see figures 2(a) and (b)). The dissipated energy is calculated from the reconstructed force–distance curves (see figure 3(a)). As discussed below, once the force parameters are fixed, the model is able to reproduce all the experimental energy dissipation data for both regimes.

4. Results

A schematic illustration of the tip–T6 interface and the experimental measurements is given in figure 1. The atomistic drawings (figure 1(a) and (b)) reflect the results of *ab initio* simulations. The AFM energy dissipation maps show several T6 monolayer islands deposited on (100)-oriented silicon wafer (figure 1(c)). The Si surface is covered by a silicon dioxide film of about 6 Å. The energy dissipation histogram shows two peaks (see figure 1(d)). Each point used to build the histogram represents a single energy measurement. The lower peak is associated with energy dissipation on the silicon while the other is associated with energy dissipation on the T6. The full width at half-maximum is 0.2 eV and 0.3 eV, respectively. The measurements have been performed in a non-invasive manner since actual energy dissipated per bond is about one order of magnitude smaller than the bond energy. We have measured the energy dissipated as 2.10 eV and 2.45 eV for silicon and T6, respectively. The measurements have been performed in the attractive regime with $A/A_0 = 0.92$ ($A_0 = 15.6$ nm, $k = 1.7$ N m^{-1} and $Q = 159$).

Figure 2 shows the experimental steps to measure the dissipated energy as a function of the amplitude. Figures 2(a) and (b) display the amplitude and phase-shift curves for both attractive and repulsive regimes, respectively. We note that the data shown in figures 1 and 2 correspond to different experiments. The dissipated energy can be calculated by the equation [35]

$$E_{\mathrm{dis}} = \frac{\pi k A}{Q}\left(A_0 \sin\phi - \frac{A\omega}{\omega_0}\right), \tag{2}$$

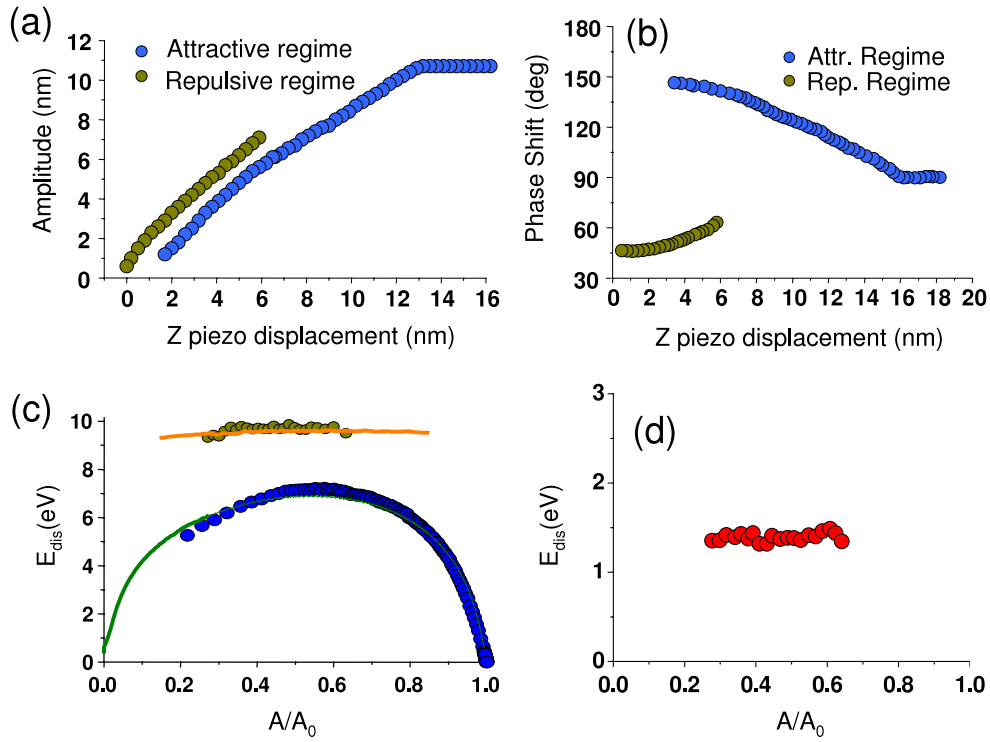

Figure 2. (a) Experimental amplitude versus tip–surface distance curves. Two branches, one for the tip–surface repulsive interaction regime and the other one for the attractive regime, are shown. (b) Phase-shift versus distance curves for the same experimental run. (c) Energy dissipation dependence on the normalized oscillation amplitude. The experimental curves (dots) are faithfully reproduced by a point-mass simulation that uses DMT contact mechanics and van der Waals forces (solid lines). (d) Experimental energy dissipated by short-range repulsive forces.

where Q and k are the quality factor and force constant of the cantilever ($Q = 300$ and $k = 12$ N m^{-1}); A_0 is the free amplitude ($A_0 = 11$ nm), ϕ is the phase shift between the excitation and the tip response while ω_0 and ω are the first resonance and excitation frequencies (here, $\omega_0 = \omega$). The values determined from equation (2) are shown in figure 2(c). The dissipated energy is larger in the repulsive regime because the integral of the force versus tip–surface displacement (see figures 3(a) and (b)) is larger [9]. The experimental curves in both regimes can be reproduced by our point-mass model dynamical simulations including DMT contact mechanics and van der Waals attractive forces (see figure 2(c)), with parameters adjusted to fit a single experimental point (A_i, ϕ_i). We have a very good description of the energy dissipation curves with effective elastic moduli $Y^* = 170$ GPa and 60 GPa for silicon and T6, respectively, and $\alpha_a = 7 \times 10^{-28}$ J m, $\gamma_a = 50$ mJ m^{-2}, $\alpha_r = 3\alpha_a$ and $\gamma_r = 57$ mJ m^{-2} for the interaction during approach and retraction. The tip radius is $R = 7$ nm.

Dissipation at the nanoscale is described in terms of the surface adhesion hysteresis [9, 36]. It might come from long-range interactions and/or from short-range atomic and molecular interactions. Compositional contrast could be obtained in both ranges, although that achieved in the repulsive regime is usually sharper. The contrast in the attractive regime could also have a residual contribution from capillary forces [37]. For this reason we focus on the repulsive regime to perform quantitative comparison between experiments and first-principles calculations.

Figure 3 shows the force versus distance curve that describes the experimental results shown in figure 2. The curves have been reconstructed by using the contact mechanics model described above. The hysteresis observed between the loading and uploading of the tip gives rise to energy dissipation. The force–distance curve shows that, in the repulsive regime, there are contributions from both short- and long-range dissipation effects (see figure 3(a)). Theoretical curves show that the measurements performed in the repulsive regime contain contributions from both short- and long-range dissipation effects (see figure 3(b)). On the other hand, because the minimum tip–surface distance in the attractive regimes is about 3 Å (see figure 3(c)), the attractive regime gives only partial information about long-range dissipative processes. The shaded region in figure 3(b) remains unexplored in the attractive regime. However, the excellent agreement obtained between point-mass simulations and experiments (see figure 2(c)) allows us to determine the energy dissipated in the shaded area. Thus, to determine the energy dissipated exclusively through short-range interaction forces (E_{sr}), we subtract from the energy measured in the repulsive regime (E_r) the energy dissipated through long-range forces (E_a) and energy dissipated in the shaded area (E_{sh}). Then the energy dissipated by short-range forces, $E_{sr} = E_r - E_a - E_{sh}$, is 1.4 eV (see figure 2(d)), with an absolute error bar, determined by a conservative estimate of the experimental uncertainty in the measurement of the amplitude and phase of 0.6 eV.

By using first-principles simulations we investigate the atomic and molecular mechanisms responsible for the energy

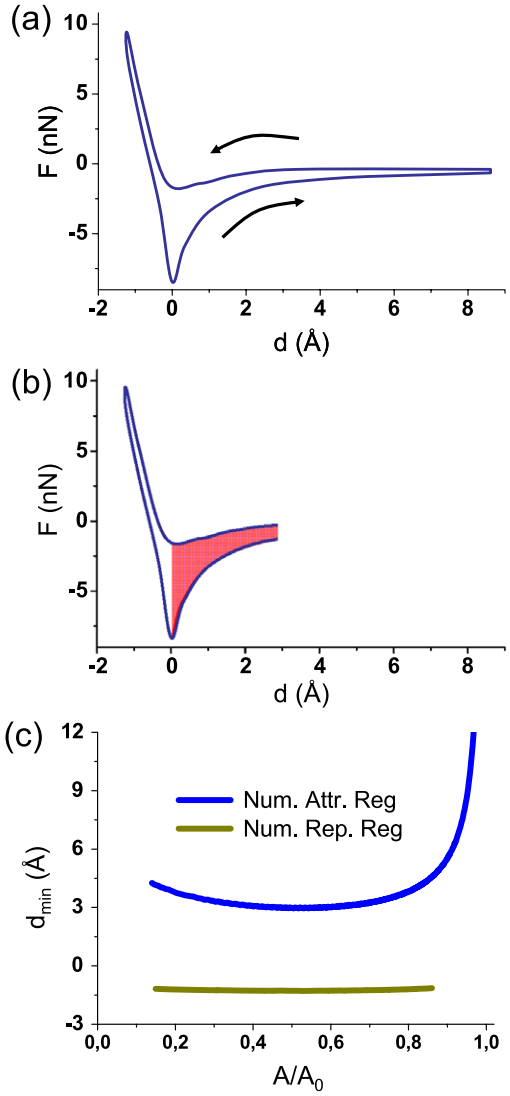

Figure 3. (a) Force–distance curve reconstructed from the experiments shown in figure 2. Arrows indicate the loading and unloading sections. (b) Force–distance curve difference between the repulsive and attractive regimes. The shaded region remains experimentally unexplored in the attractive regime because the minimum distance is about 3 Å (c). Minimum tip–surface distance for the simulation shown in figure 2(c). In the attractive regime the turning point is 3 Å above the surface while in the repulsive regime the tip penetrates 1.4 Å into the T6 layer.

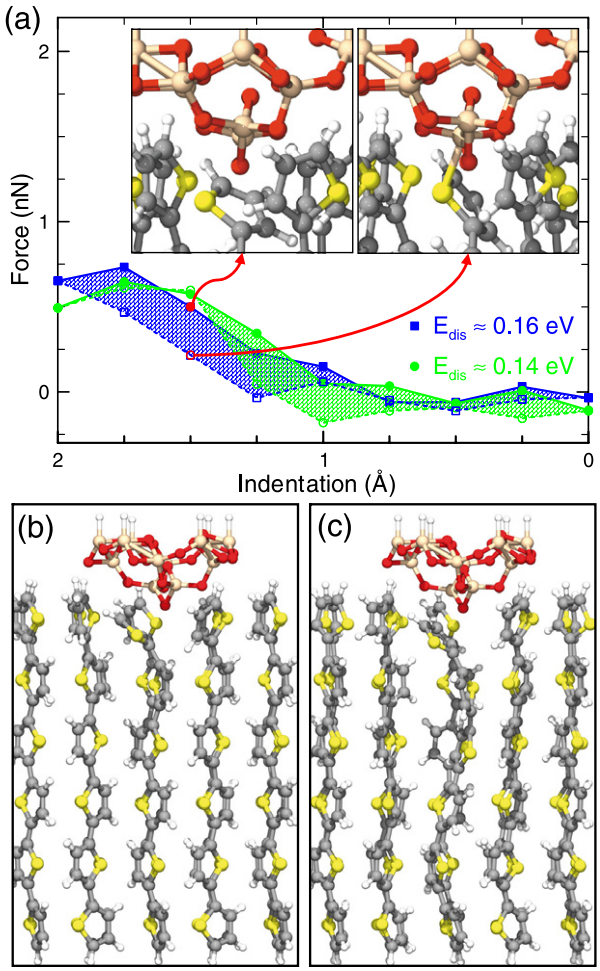

Figure 4. (a) Force–distance curves at a hollow position between molecules (green, circles) and over a sulfur atom (blue, squares). The curves show the approach (full symbols) and retraction (empty symbols) components. The insets display the thermal-averaged atomic coordinates for the same tip–sample distance in approach (left) and retraction (right) half-cycles for S position of the tip. (b) Side view of the tip–T6 interface at 0 K. The forces produce the rotation of a thiophene unit and the bond contraction along the chain. (c) Side view of the tip–T6 interface at 300 K. The system relaxes by propagating a deformation along the molecular chain.

dissipation. Figure 4(a) shows two force–distance curves indenting up to 2 Å calculated on top of a sulfur atom and in a hollow site between the molecules at 300 K. The curves depend on history (loading versus unloading), temperature and the tip position with respect to the T6 cell. When the tip is on a hollow position, most of the energy is dissipated during the first half of the indentation while on an S position the hysteresis occurs at the end of the indentation (see figure 4(a)). However, the values of the dissipated energies are very similar, 0.16 versus 0.14 eV. There is always an uncertainty in matching the contact point defined for the ideally flat surface assumed in the continuum mechanics approach with the real, atomistic description considered in the *ab initio* simulations. This is why we have not limited our analysis to the indentation distance extracted from the continuum mechanics, but have explored a larger distance range in order to determine the possible influence of this parameter in the dissipated energy. From the results of figure 4(a) it is already clear that, for the hollow position (green curve), there is no change in the dissipated energy if we retract the tip from an indentation distance of 1.5 Å. In the case, of the S position (blue curve), there would be a small reduction, but there is no qualitative change in the magnitude of the dissipated energy or the molecular mechanism responsible for the hysteresis discussed below.

The deformation mechanisms are local. They involve significant distortions only in the very few molecules closest to the tip (see figures 1 and 4). The molecules could accommodate the load through compression of molecular bonds, rotation of the thiophene subunits (see figure 4(c)) and

bending of the whole chain (see folding modes in figure 4(c)). The competition among these modes is crucial for the accurate determination of tip–sample forces under room temperature operation. At $T = 0$ K the folding modes are frozen. The system is trapped in some high-stress local minima where the mechanical response is dominated by bond compression (see figure 4(b)). The quasi-static approach ($T = 0$ K), when the atoms in the molecular layer and the tip are allowed to relax to their ground-state configuration at each step of the approach/retraction curves, does not capture the mechanical response of the system. By increasing the temperature, the folding modes become active and the above high-stress structures evolve into states with significantly lower repulsive forces.

The simulations confirm that at 300 K the folding modes (see figure 4(c)) are very efficient in reducing the repulsive interactions in the first stages of the indentation process. The strong repulsive regime (indentations up to 5 Å, not shown) is actually well described by the computationally much faster quasi-static $T = 0$ K approach. These calculations provide the mechanical strength in the first stages of the indentation process in good agreement with the results obtained from the continuum modelling of the experimental force–distance curves.

The hysteresis can be explained in terms of the energy landscape of metastable molecular configurations that the system can adopt for a given tip position. The insets of figure 4(a) show the thermal-averaged atomic coordinates for the same tip–sample distance in approach and retraction half-cycles. Notice that the bonds formed during further indentation from this tip–sample distance control the adhesive response in the retraction stage. The system is trapped, due to the presence of energy barriers that cannot be overcome even with the available thermal energy, in different bonding configurations corresponding to local energy minima during the approach and retraction of the tip. These energy barriers are responsible for breaking the adiabaticity and thus lead to energy dissipation.

The adhesion hysteresis discussed above is compatible with structurally reversible processes. It states that, for a given tip–surface distance, there is a unique potential energy surface. This surface has several local minima with respect to the atomic positions. The hysteresis appears because the observable atomic positions do depend on the history of the tip motion. The mechanism is similar to the Tomlinson model invoked to introduce atomic-scale friction [38].

Next, we compare the above result with the energy dissipation measured from the experiments. The experimental contact area can be determined by contact mechanics models using the expression that links indentation values δ and tip radius R with the contact radius $a = \sqrt{\delta R}$, where $\delta = 1.4$ Å (see figure 3(c)) and $R = 7$ nm (the value used in figure 2(c) to compare with the experiment). A multiasperity contact is expected in the contact area ($\sim \pi a^2 = 3.1$ nm^2) which is large compared to each individual molecular contact for a single nano-asperity used in the molecular dynamics simulations. Then, we can estimate a contact radius around 3.5 Å for a 2 Å indentation. We have shown that deformation mechanisms are very local and the dissipated energy is very similar for the different tip positions. Thus, we can simply scale up the molecular contacts $\sim$0.4 nm^2 to the experimental contact area $\sim$3.1 nm^2 (about eight molecular contacts, see figure 5). Then, the experimental value $\sim$1.4 eV is in good agreement with the data inferred from first-principles simulations, namely $1.2\ \text{eV} = 8 \times 0.15$ eV.

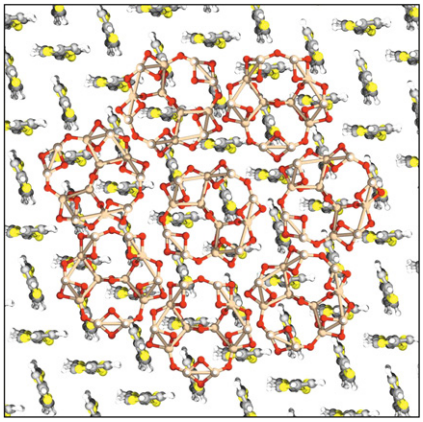

Figure 5. Atomistic representation of the tip–T6 interaction area deduced from experiments and contact mechanics simulations in terms of the silica tips used in the first-principles simulations.

The shape of the force–distance curves (see figure 4(a)) depends on the atomic position: however, this dependence is irrelevant when the dissipated energy is considered. Then, by averaging the dissipation energy values we can describe the experimental data taken with a silicon tip covered by a native oxide, where the structure of the silicon oxide at the very end of the tip is amorphous.

5. Conclusions

The presented results show that the contrast observed in phase images of T6 molecules can be explained by reversible atomic and molecular reorganization processes. Those processes involve different equilibrium positions for the atoms interacting with the tip during the loading and unloading cycles. Due to the presence of energy barriers between these local minima, the configuration space sampled by the tip depends on the direction of the tip motion. Individual processes involve maximum forces of about 1 nN which do not produce irreversible changes in the molecular structure of the T6 chains. This work sheds light on the mechanical deformations induced during imaging and the atomistic mechanisms that are responsible for the energy dissipation observed in the AM-AFM experiments, and supports the use of AM-AFM phase-imaging as a tool for quantitative analysis of materials with high spatial resolution in relevant air and liquid environments.

Acknowledgments

This work was financially supported by the European Commission (FORCETOOL, NMP4-CT-2004-013684), the Spanish Ministry of Science and Innovation (MICINN) under

projects MAT2006-038339 and MAT2008-02929-NAN and the ESF EUROCORES FANAS Programme (AFRI Project, MAT2008-02939-E).

References

[1] Möller C, Allen M, Elings V, Engel A and Müller D J 1999 *Biophys. J.* **77** 1150–8
[2] Stroh C, Wang H, Bash R, Ashcroft B, Nelson J, Gruber H, Lohr D, Lindsay S M and Hinterdorfer P 2004 *Proc. Natl Acad. Sci. USA* **101** 12503–7
[3] Yokokawa M, Wada C, Ando T, Sakai N, Yagi A, Yoshimura S H and Takeyasu K 2006 *EMBO J.* **25** 4567–76
[4] Klinov D and Magonov S 2004 *Appl. Phys. Lett.* **84** 2697–9
[5] García R, Magerle R and Pérez R 2007 *Nat. Mater.* **6** 405–11
[6] Xu J, Guo B H, Zhang Z M, Zhou J J, Jaing Y, Yan S, Li L, Wu Q, Chen G Q and Schultz J M 2004 *Macromolecules* **37** 4118–23
[7] Tsarkova L, Knoll A and Magerle R 2006 *Nano Lett.* **6** 1574–7
[8] Suo Z, Yang X, Avci R, Kellerman L, Pascual D W, Fries M and Steele A 2007 *Langmuir* **23** 1365–74
[9] García R, Gómez C, Martínez N F, Patil S, Dietz C and Magerle R 2006 *Phys. Rev. Lett.* **97** 016103
[10] Anczykowski B, Gotsmann B, Fuchs H, Cleveland J P and Elings V B 1999 *Appl. Surf. Sci.* **140** 376–82
[11] Martin P, Marsaudon S, Aimé J P and Bennetau B 2005 *Nanotechnology* **16** 901–7
[12] Loppacher C, Bennewitz R, Pfeiffer O, Guggisberg M, Bammerlin M, Schär S, Barwich V, Baratoff A and Meyer E 2000 *Phys. Rev.* B **62** 13674–9
[13] Meyer E, Howard L, Overney R M, Heinzelmann H, Frommer J, Güntherodt H J, Wagner T, Schier H and Roth S 1991 *Nature* **349** 398–400
[14] Hug H J and Baratoff A 2002 *Noncontact Atomic Force Microscopy* (Berlin: Springer) chapter 20, pp 395–432
[15] Oyabu N, Pou P, Sugimoto Y, Jelínek P, Abe M, Morita S, Pérez R and Custance O 2006 *Phys. Rev. Lett.* **96** 106101
[16] Sugawara Y, Kobayashi N, Kawakami M, Li Y J, Naitoh Y and Kageshima M 2007 *Appl. Phys. Lett.* **90** 194104
[17] Fukuma T and Jarvis S P 2006 *Rev. Sci. Instrum.* **77** 043701
[18] Uchihashi T, Ando T and Yamashita H 2006 *Appl. Phys. Lett.* **89** 213112
[19] Paulo A S and García R 2002 *Phys. Rev.* B **66** 041406
[20] Lee M and Jhe W 2006 *Phys. Rev. Lett.* **97** 036104
[21] Hölscher H and Schwarz U D 2007 *Int. J. Non-Linear Mech.* **42** 608
[22] Hu S and Raman A 2007 *Appl. Phys. Lett.* **91** 123106
[23] Loi M A, Da Como E, Dinelli F, Murgia M, Zamboni R, Biscarini F and Muccini M 2005 *Nat. Mater.* **4** 81–5
[24] Samorí P and Rabe J P 2002 *J. Phys.: Condens. Matter* **14** 9955–73
[25] Porzio W, Destri S, Mascherpa M and Brueckner S 1993 *Acta Polym.* **44** 266
[26] Horowitz G, Bachet B, Yassar A, Lang P, Demanze F, Fave J L and Garnier F 1995 *Chem. Mater.* **7** 1337
[27] Moulin J F, Dinelli F, Massi M, Albonetti C, Kshirsagar R and Biscarini F 2006 *Nucl. Instrum. Methods Phys. Res.* B **246** 122
[28] Telesca R, Bolink H, Yunoki S, Hadziioannou G, Duijnen P T V, Snijders J G, Jonkman H T and Sawatzky G A 2001 *Phys. Rev.* B **63** 155112
[29] Sader J E, Chon J W M and Mulvaney P 1999 *Rev. Sci. Instrum.* **70** 3967
[30] Jelínek P, Wang H, Lewis J P, Sankey O F and Ortega J 2005 *Phys. Rev.* B **71** 235101
[31] Basanta M A, Dappe Y J, Jelínek P and Ortega J 2007 *Comput. Mater. Sci.* **39** 759–66
[32] Kohn W and Sham L J 1965 *Phys. Rev.* **140** A1133–8
[33] Bromley S T, Zwijnenburg M A and Maschmeyer T 2003 *Phys. Rev. Lett.* **90** 035502
[34] Derjaguin B V, Muller V M and Toporov Y P 1975 *J. Colloid Interface Sci.* **53** 314–26
[35] Martinez N F and García R 2006 *Nanotechnology* **17** S167
[36] Yoshizawa H, Chen Y L and Israelachvili J 1993 *J. Phys. Chem.* **97** 4128
[37] Sahagún E, García-Mochales P, Sacha G M and Sáenz J J 2007 *Phys. Rev. Lett.* **98** 176106
[38] Giessibl F J, Herz M and Mannhart J 2002 *Proc. Natl Acad. Sci. USA* **99** 12006–10